16th World Conference on Earthquake, 16WCEE 2017

Santiago Chile, January 9th to 13th 2017

Paper N° 142

Registration Code: S-N1462924128

SEISMIC PERFORMANCE OF A HIGH VOLTAGE TRANSFORMER-BUSHING SYSTEM

G L. Ma(1), JY Wen(2), R Y. Zhu(3), Q. Xie(4)

(1)*PhD. Candidate, Department of Structural Engineering, Tongji University, mgldut@163.com*
(2) *PhD. Candidate, Department of Structural Engineering, Tongji University, 519272118 @qq.com*
(3) *Engineer, Electric Power Planning & Engineering Institute, zhuruiyuan2429@163.com*
(4) *Professor, Department of Structural Engineering, Tongji University, qxie@tongji.edu.cn*

Abstract

To investigate seismic performance of 220kV transformer-bushing systems, a small transformer tank was designed and manufactured, and equipped with 2 real 252 kV porcelain bushings. Shaking table tests on the transformer-bushing system were conducted. Modal properties were acquired through white-noise scanning tests. Seismic performance of the transformer-bushing system under Wenchuan earthquake ground motion excitation was also acquired. The tests show that the transformer tank and turret significantly amplify acceleration at the flanges of the bushings, whereas displacement, strain responses are acceptable. Rocking vibration of the bushing-turret assembly induced by flexibility and out-of-plane bending vibration of tank wall markedly magnifies bushing seismic responses. The earthquake responses of the bushings remarkably couples with rocking vibration of the turret.

Keywords: *transformer-bushing system, shaking table tests, rocking vibration*

1. Introduction

Power grid is one of lifeline engineering infrastructures that play a vital role in modern society. When the distance between the generating station and the load end is large in power grid, it is essential to step up the electricity voltage at the generating station and step it down at the load end since a high voltage transmission line carries less current and thus has fewer losses with the same power demand and conductor size. It is the power transformer installed in a substation that transforms voltage ratings in the power grid. Transformers have exhibited vulnerable seismic performance during recent earthquakes worldwide, including the 2008 Wenchuan and 2013 Lushan earthquakes in China [1, 2], the 2010 Chile earthquake [3], the 2010 Baja California earthquake in Mexico [4], the 2010 Haiti earthquake [5], the 2010-2011 Canterbury earthquakes in New Zealand [6], and the 2011 Tohoku earthquake in Japan [7]. During these earthquakes, high voltage transformers sustained various severe damages such as overturning from the foundation, porcelain bushing fracture, oil leakage, and so on[8]. Hence, it is imperative to evaluate and improve seismic performance of high voltage transformer-bushing system.

Considerable studies[8-14] on seismic performance of transformers or bushings were carried out as per the IEEE693-2005 Standard[15]through shaking table tests or finite element analyses. The IEEE693-2005 Standard recommends the seismic qualification method—shaking table test on high voltage transformer bushings fixed on a rigid stand in lieu of the transformer tank as it is impractical to test a real high voltage transformer-bushing system on a shaking table. Besides, the IEEE693-2005 Standard considers that the motion at the flange of the bushing is equal to the ground motion multiplied by a frequency-independent magnification factor of 2 becuse the motions that the bushing experiences from the ground motions are amplified due to the flexibility of the transformer tank and turret. Shaking table tests of porcelain bushings on a rigid stand as per the IEEE693-2005 seismic qualification procedure had demonstrated a generally good performance of transformer bushings. However, these results were not consistent with the actual vulnerable performance of transformer-bushings system during the recent earthquakes. It was suspected that the actual seismic performance of porcelain bushing may be aggravated by the flexibility of bushing supporting structures, such as the tank and turret. More tests on the transformer and bushing as a whole system are needed to shed light on its seismic performance.

This study conducted shaking table tests on a high voltage transformer-bushing system, with a particular focus on earthquake response mechanism of transformer bushings mounted on a transformer tank and the magnitude of potential dynamic amplification effect for transformer bushings.

2. The Transformer-bushing System

The prototype of the transformer-bushing system is a single phase 220 kV transformer, which is commonly used in high voltage substations in China. A typical transformer usually consists of a tank, iron cores and coils, porcelain or composite bushings with different voltage ratings, an oil conservator, and other accessories. Considered the geometric size of the prototype transformer and payload of the shaking table, the transformer tank was scaled and designed by authors and manufactured by a transformer manufacturer-*TBEA*. As shown in Figure 1. (a), the transformer-bushing system used for shaking table tests was composed of a transformer tank, two turrets of different types separately protruding from the top plate and side wall of the tank (hereafter referred to as **TT** and **ST**, respectively), two commercial 252kV porcelain bushings (mechanically clamped type) installed on the turrets (bushings mounted on **TT** and **ST** turrets are referred to as **TB** and **SB**, respectively), and an oil conservator mounted above one end of the tank. Properties of the transformer-bushing system model is tabulated in table 1. In addition, the ferrous cores and coils were not included in the system because they were firmly fixed to the tank bottom plate. The tank was designed so that it represented the actual transformer structural configuration and the fundamental frequency of the single phrase transformer-bushing system. The latter was achieved by tentative computation using finite element analysis during design stage.

For ease of reference, the transversal direction of the transformer tank was defined as *X* direction, which was also the main excitation direction for shaking table tests; the longitudinal and vertical directions of the tank were defined as *Y* and *Z* directions, respectively. The transformer-bushing system installed on the shaking table is shown in Figure 1(a).

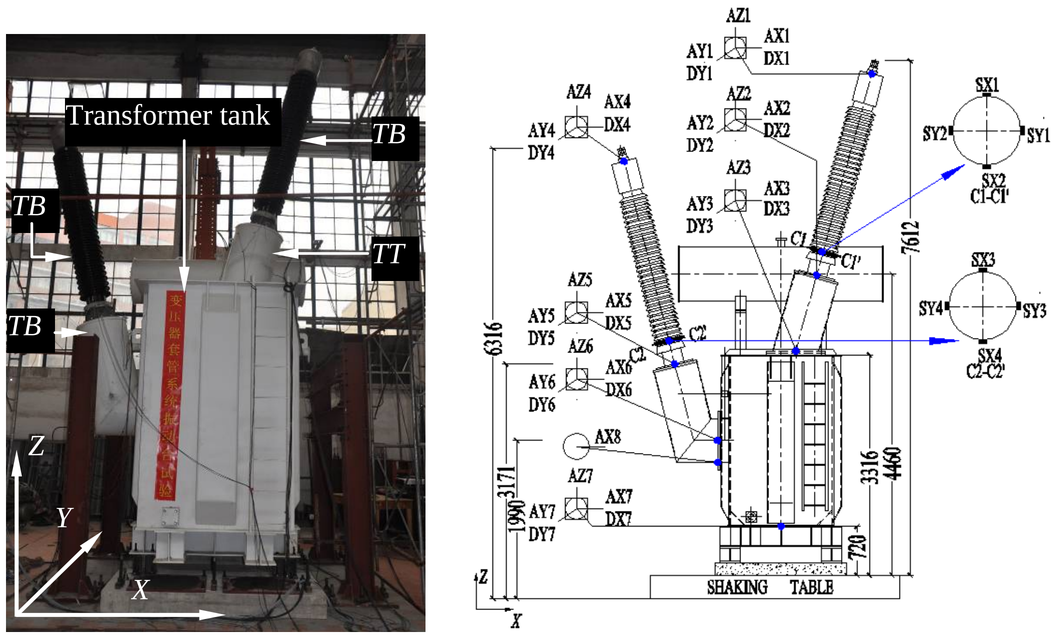

(a) Panoramic view (b) Dimensions and instrumentation arrangement

Figure 1. The transformer-bushing system (units: mm)

Table 1- Properties of the transformer-bushing system

	Bushing	Transformer
Material	Porcelain	Steel
Voltage rating	252 kV	
Total length	5.12 m	
Length above bushing flange	2.61 m	
Maximum diameter	270 mm	
Total mass*	620 kg	20 000 kg
Width×length×height		1.5 m×2.9 m×2.5 m
Diameter of turrets		ϕ 640 mm
Diameter×length of oil conservator		ϕ 0.8m×3 m
Wall thickness		12 mm(tank bottom plate:30mm)
Stiffer thickness		6 mm

*For transformer, including the watered tank and the oil conservator, two bushings with turrets, and footing concrete pads.

3. TEST PROTOCOL

3.1 Earthquake inputs

A total of three sets of Wenchuan earthquake ground motions: Wolong, Qingping and Zengjia records, were selected as table earthquake inputs for the tests because hundreds of high voltage transformers of this type were damaged in the great Wenchuan Earthquake. More detailed earthquake ground motion is reported in literature [16].

3.2. Instrumentation

The experimental data were collected using an automatic data acquisition system at 256 Hz in 96 channels.

Figure 1 (b) displays the dimensions and instrumentation of the system for shaking table test, where A, D and S stand for sensors for acceleration, displacement and strain measurements, and *X*, *Y*, and *Z* for seismic response direction. A total of 42 sensors were instrumented to the system. 22 accelerometers were used to measure accelerations at the top, mounting flanges of bushings (TB and SB), bottom of turrets (TT and ST), and bottom of the tank in *X*, *Y*, *Z* directions. 12 displacement transducers were fixed at the tops and flanges of the bushings, the tops and bottoms of the tank to measure displacements in *X*, and *Y* directions. 4 strain gauges were mounted at the root of upper porcelain unit of each bushing to acquire porcelain strain responses in *XZ* plane and *YZ* plane. The instrumentation is shown in figure 1.(b), □ stands for accelerometers,○ for displacement transducers, ▄ for strain gauges, AX/Y/Z×, DX/Y× and SX/Y ×show accelerometer, displacement transducer, strain gauge, measuring direction and number.

3.3. Test program

The tests were designed with three stages in which the system was excited by the three earthquake records in *X*/*Y*, *XY*, *XYZ* directions with PGAs of 0.1g, 0.2g and 0.4g representing low, moderate and high design intensity 8 in China. The table main excitation direction was *X*, the peak accelerations in *Y*, *Z* direction were corrected as: $a_y = 0.85a_x$, $a_z = 0.65a_x$ where a_x , a_y , a_z represents peak accelerations in direction *X*, *Y* and *Z*, respectively.

Table 2 summarizes the tests containing 39 cases. In low/moderate/high cases, 12 cases of tests were carried out on the system. In addition, white-noise scanning tests (WN1/2/3) were performed to identify the modal behavior of the system at the beginning of low/moderate/high cases. In the Table case label columns, the first capital letters ‘W’, ‘Q’, and ‘Z’ denote table input motions-Wonglong, Qingping, and Zengjia records respectively; the following two capital letters ‘UX’,‘UY’,‘BI’,‘TR’ indicate the shaking table excited uni-axially in *X* or *Y* direction, bi-axially in *X* and *Y* directions, tri-axially in *X*, *Y* and *Z* directions; and the remaining numerals and letter ‘0.1g’, ‘0.2g’, ‘0.4g’ signify the peak ground accelerations of the main excitation direction.

Table 2- Program of the tests

Low PGA				Moderate PGA				High PGA			
Case label	Measured PGA (g)			Case label	Measured PGA (g)			Case label	Measured PGA (g)		
	X	*Y*	*Z*		*X*	*Y*	*Z*		*X*	*Y*	*Z*
WN1	0.028	0.039	−	WN2	0.034	0.032	−	WN3	0.033	0.040	−
WUX0.1g	0.130	—	—	WUX0.2g	0.275	—	—	WUX0.4g	0.529	—	—
WUY0.1g	—	0.117	—	WUY0.2g	—	0.217	—	WUY0.4g	—	0.504	—
WBI0.1g	0.131	0.094	—	WBI0.2g	0.275	0.190	—	WBI0.4g	0.543	0.432	—
WTR0.1g	0.131	0.099	0.071	WTR0.2g	0.250	0.220	0.148	WTR0.4g	0.506	0.482	0.343
QUX0.1g	0.103	—	—	QUX0.2g	0.219	—	—	QUX0.4g	0.461	—	—
QUY0.1g	—	0.106	—	QUY0.2g	—	0.229	—	QUY0.4g	—	0.454	—
QBI0.1g	0.106	0.092	—	QBI0.2g	0.239	0.206	—	QBI0.4g	0.454	0.451	—
QTR0.1g	0.150	0.090	0.070	QTR0.2g	0.270	0.204	0.187	QTR0.4g	0.490	0.402	0.303
ZUX0.1g	0.129	—	—	ZUX0.2g	0.251	—	—	ZUX0.4g	0.528	—	—
ZUY0.1g	—	0.110	—	ZUY0.2g	—	0.239	—	ZUY0.4g	—	0.556	—
ZBI0.1g	0.131	0.092	—	ZBI0.2g	0.265	0.197	—	ZBI0.4g	0.553	0.449	—
ZTR0.1g	0.129	0.097	0.064	ZTR0.2g	0.267	0.214	0.131	ZTR0.4g	0.514	0.440	0.283

4. RESULTS OF THE SHAKING TABLE TESTS

4.1 Dynamic properties of the transformer-bushing system

At the beginning of each stage tests, the system was scanned using white noise (WN1in Table 2) with frequency ranging from 0.1 to 50 Hz bi-axially to identify its natural frequencies and corresponding damping ratios. The first natural frequencies of the system in each direction were obtained from the most prominent peaks in amplitude spectra of acceleration transfer functions at the top of the each bushing. The related modal equivalent viscous damping ratios were estimated by means of the half-power band-width method applied to the peaks in the amplitude spectra. Table 3 lists the first natural frequencies and related damping ratios in each direction.

Table 3. Modal properties of the system

Bushing	Direction	Natural frequencies (Hz)	Equivalent damping ratios (%)
TB	*X*	5.58	1.5
	Y	5.74	2.7
SB	*X*	5.04	2.1
	Y	6.00	3.3

4.2. Results of seismic responses

Tables 4-6 list the main results of the tests. Each case varying from input ground motion to its PGA, the tables contain the following data: (1) acceleration amplification factor (*AAF*); (2) peak relative displacements at tops of bushings to transformer bottom; and (3) peak strain responses at roots of upper porcelain units of the bushings. *AAF* is a comprehensive index that reflects magnifying effect of the transformer tank and turret to the input earthquake acceleration at a bushing flange level. Both the IEEE693-2005 and GB50260-2013 [17] suggest that the *AAF* at the flange level of a bushing be defined as:

$$AAF = \frac{\max(|a_{Bfla}|)}{\max(|a_{Tbot}|)} \tag{1}$$

Where a_{Bfla} is the time history of acceleration at the flange of the bushing; a_{Tbot} is the time history of earthquake acceleration at the transformer bottom; and $\max(|\cdot|)$ is the maximum absolute value of the time histories. Stain responses of the bushings at bottom of upper porcelain unit were regarded as an essential parameter to assess whether the porcelain unit would crack.

Table 4. Results of seismic tests

Case label	*AAF*						Peak displacement (mm)				Peak bending strain (10^{-6})			
	TB			SB			TB		SB		TB		SB	
	X	*Y*	*Z*	*X*	*Y*	*Z*	*X*	*Y*	*X*	*Y*	*X*	*Y*	*X*	*Y*
WUX0.1g	1.69	—	—	1.57	—	—	4.86	—	4.77	—	24.42	—	34.85	—
WUY0.1g	—	2.38	—	—	1.54	—	—	9.34	—	8.17	—	47.95	—	39.48
WBI0.1g	1.56	2.42	—	1.43	1.70	—	6.15	7.30	5.91	7.01	30.36	36.62	35.12	32.88
WTR0.1g	3.40	2.96	2.73	2.29	2.55	1.57	8.37	7.51	5.35	5.95	42.42	38.56	35.89	39.68
QUX0.1g	1.89	—	—	2.47	—	—	3.93	—	3.84	—	23.78	—	21.85	—
QUY0.1g	—	1.66	—	—	1.63	—	—	4.50	—	3.81	—	28.37	—	23.27
QBI0.1g	1.58	1.76	—	2.30	1.82	—	3.32	4.56	3.08	2.86	20.44	27.09	22.86	15.50
QTR0.1g	2.75	3.04	2.39	3.15	2.44	1.92	3.89	4.26	3.51	2.47	26.03	21.84	25.35	27.84
ZUX0.1g	1.77	—	—	1.43	—	—	4.84	—	4.61	—	21.42	—	35.56	—
ZUY0.1g	—	1.45	—	—	1.22	—	—	3.70	—	3.40	—	19.92	—	20.19
ZBI0.1g	1.80	1.69	—	1.55	1.36	—	4.52	4.32	4.35	4.07	21.70	20.92	35.90	25.07
ZTR0.1g	1.71	1.92	1.58	1.75	1.37	1.29	5.24	5.18	6.05	2.92	24.83	21.81	29.34	21.86

Table 5. Results of seismic tests

Case label	*AAF*						Peak displacement(mm)				Peak bending strain (10^{-6})			
	TB			SB			TB		SB		TB		SB	
	X	*Y*	*Z*	*X*	*Y*	*Z*	*X*	*Y*	*X*	*Y*	*X*	*Y*	*X*	*Y*
WUX0.2g	1.62	—	—	1.57	—	—	11.99	—	11.72	—	57.03	—	83.03	—
WUY0.2g	—	2.12	—	—	1.44	—	—	19.05	—	14.01	—	94.63	—	54.43
WBI0.2g	1.67	2.01	—	1.48	1.42	—	16.80	14.77	16.31	12.65	87.62	76.41	83.13	53.24
WTR0.2g	2.92	2.05	2.47	1.94	1.84	1.85	14.32	15.79	12.36	11.65	70.32	70.33	62.86	75.73
QUX0.2g	1.51	—	—	2.16	—	—	7.58	—	7.34	—	45.72	—	49.28	—
QUY0.2g	—	1.24	—	—	1.55	—	—	9.01	—	7.77	—	57.03	—	41.95
QBI0.2g	1.30	1.43	—	1.97	1.39	—	8.09	8.07	7.59	7.19	44.50	45.49	41.54	47.49
QTR0.2g	2.71	2.51	3.07	3.52	2.25	1.47	7.56	8.14	7.31	4.59	52.15	48.73	52.47	49.38
ZUX0.2g	1.74	—	—	1.53	—	—	11.02	—	10.56	—	45.45	—	77.11	—
ZUY0.2g	—	1.46	—	—	1.26	—	—	7.60	—	8.52	—	39.61	—	44.93
ZBI0.2g	1.66	1.84	—	1.67	1.35	—	10.21	11.90	10.06	11.31	50.20	59.22	67.96	47.78
ZTR0.2g	1.88	1.70	1.34	1.62	1.48	1.32	10.33	10.57	13.82	6.45	51.49	47.44	59.03	44.25

Table 6. Results of seismic tests

Case label	*AAF*						Peak displacement(mm)				Peak bending strain at base of bushing (10^{-6})			
	TB			SB			TB		SB		TB		SB	
	X	*Y*	*Z*	*X*	*Y*	*Z*	*X*	*Y*	*X*	*Y*	*X*	*Y*	*X*	*Y*
WUX0.4g	1.64	—	—	1.94	—	—	21.60	—	20.93	—	92.36	—	146.54	—
WUY0.4g	—	1.67	—	—	1.34	—	—	19.61	—	14.68	—	146.16	—	103.62
WBI0.4g	1.49	1.45	—	1.66	1.38	—	22.73	17.89	21.73	14.40	109.82	113.83	116.60	98.78
WTR0.4g	3.02	2.05	2.98	2.34	1.58	1.74	27.02	24.88	38.61	29.43	116.51	137.39	121.74	112.15
QUX0.4g	1.44	—	—	1.67	—	—	16.31	—	15.68	—	98.10	—	63.79	—
QUY0.4g	—	1.38	—	—	1.37	—	—	32.23	—	35.54	—	126.39	—	62.33
QBI0.4g	1.43	1.55	—	2.13	1.41	—	17.70	25.28	16.76	35.58	97.01	95.04	72.08	75.51
QTR0.4g	2.70	2.01	2.62	3.65	1.74	2.11	17.02	14.30	16.54	12.11	99.00	77.92	100.95	82.31
ZUX0.4g	1.55	—	—	1.77	—	—	20.26	—	18.86	—	103.13	—	171.77	—
ZUY0.4g	—	1.33	—	—	1.27	—	—	16.72	—	74.67	—	88.43	—	178.11
ZBI0.4g	1.40	1.68	—	2.79	1.42	—	22.47	23.14	22.32	74.84	117.62	101.42	198.76	134.62
ZTR0.4g	1.80	1.53	1.29	1.63	2.14	1.18	17.12	19.62	27.74	24.64	99.04	93.87	108.54	81.08

From Tables 4-6, *AAF*s range from 1.29 to 3.65, some of which have exceeded the factor of 2 stipulated by standards of *IEEE693-2005* and GB50260-2013. Moreover, the *AAF*s in vertical direction are considerable large under tri-direction earthquake excitation. This is because transformer tank and turret are made from steel plates or shells. The out-of-plane flexibility of these plates and shells easily amplifies vertical acceleration. This effect is difficult to be found during shaking table tests on bushing fixed on a rigid stand.

The majority of displacement responses at the tops of bushings are below 50 mm except for the cases of ZUY0.4g and ZBI0.4g. Strain responses at the roots of upper porcelain body of the bushings increase with the increase of PGAs with the maximum strain measuring 199 $\mu\varepsilon$.

Figure 2 demonstrates the maximum displacement response envelope curves along the height of the system. The figure suggests that: (1) displacement responses increase with the increasing PGA; (2) displacement responses of SB are larger than those of TB on the whole under the same earthquake excitation in a given direction; (3) displacement response envelope curves show two inflexion points, at the bottom of turrets and the flange of the bushings. These are especially evident under earthquake excitation with a large PGA, indicating that the distribution of equivalent rigidities along the height of system change abruptly at these points. The same observation is also made for the acceleration amplification effect where the whipping effect is so significant that displacements at the tops of bushings are much larger than other positions.

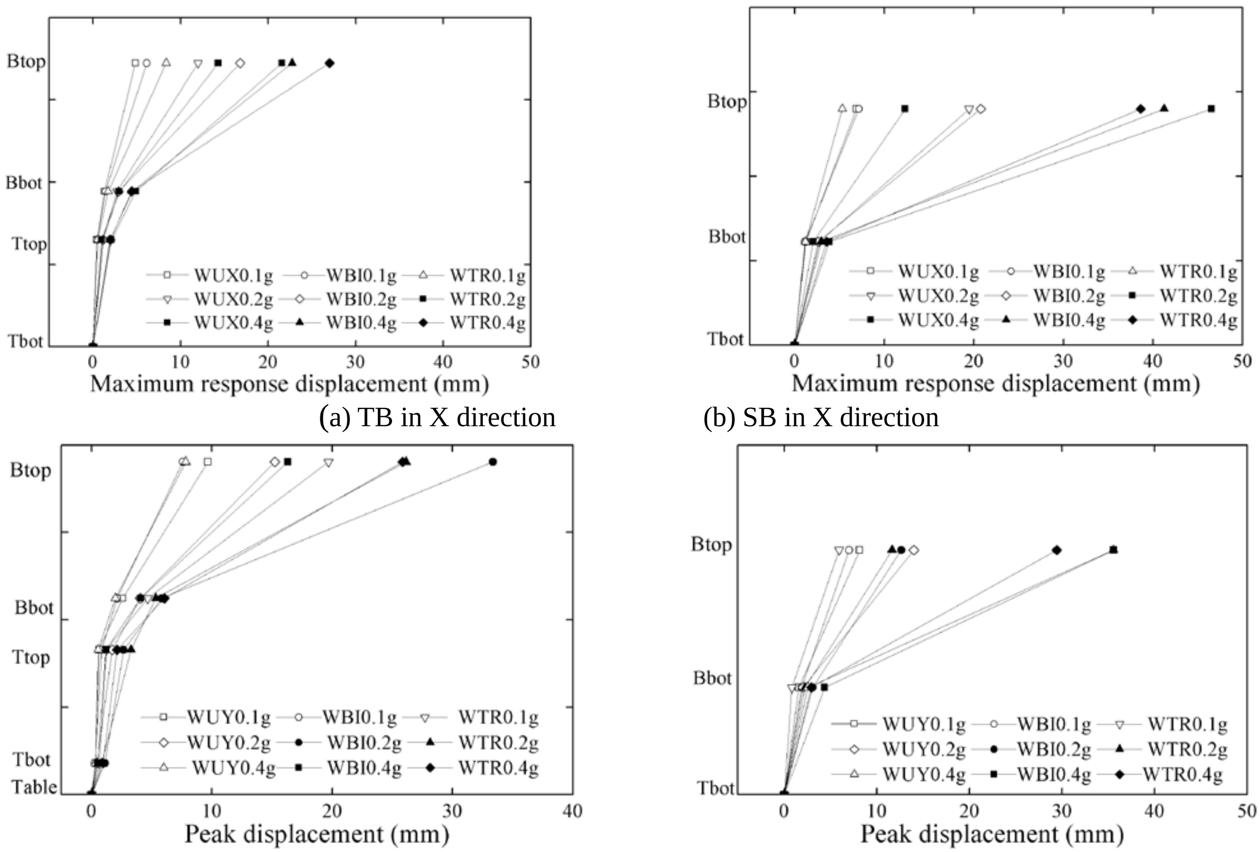

(a) TB in X direction (b) SB in X direction
(c) TB in Y direction (d) SB in Y direction

Figure 2. Displacement response envelope curves under Wolong earthquake motion excitation

5. DISCUSSION

5.1. Effect of turret type on seismic response

The white noise scanning results show that the fundamental frequencies of two 252 kV bushings installed on the transformer tank decrease significantly, among which the fundamental frequency of SB in *X* direction decreases the most, while the fundamental frequency of SB in *Y* direction decreases the least. It is believed that this difference results from the turret type effect in two directions.

Almost 1/3 of *AAF*s of TB in both *X* and *Y* directions, still 1/3 of *AAF*s of SB in *X* direction exceed 2.0, whereas all *AAF*s of SB in *Y* direction are below 2.0. *AAF*s of TB in *X* and *Y* directions, and of SB in *X* direction are larger than those of side bushing in *Y* direction. In these directions, the stiffness of turret root exerted by tank cover or side wall is weaker than that of SB in *Y* direction corresponding to a stronger stiffness of turret root exerted by tank side wall. This suggests that restraints of turret roots by tank side or cover wall have considerable influence on seismic response of a turret-bushing assembly. In fact, as shown in Figure 3, the seismic responses of TT in *X* and *Y* directions, and of ST in *X* direction are closely associated with the out-of-plane bending vibration of tank wall, which directly results in rocking vibration of turret-bushing assembly. The stiffness of ST in *Y* direction has a lot to do with the in-plane torsional vibration of tank wall. The mechanisms of the out-of-plane bending vibration and the in-plane torsional vibration of tank wall differ so greatly that they lead to differently seismic responses of the turret-bushing assembly. The stiffness of tank wall for the out-of-plane bending vibration is much lower than that for the in-plane torsional vibration, which contributes to the substantial seismic response of TB in both *X* and *Y* directions, as well as SB in *X* direction. Hence, in the following section, the effect of rocking vibration of the turret-bushing assembly is discussed.

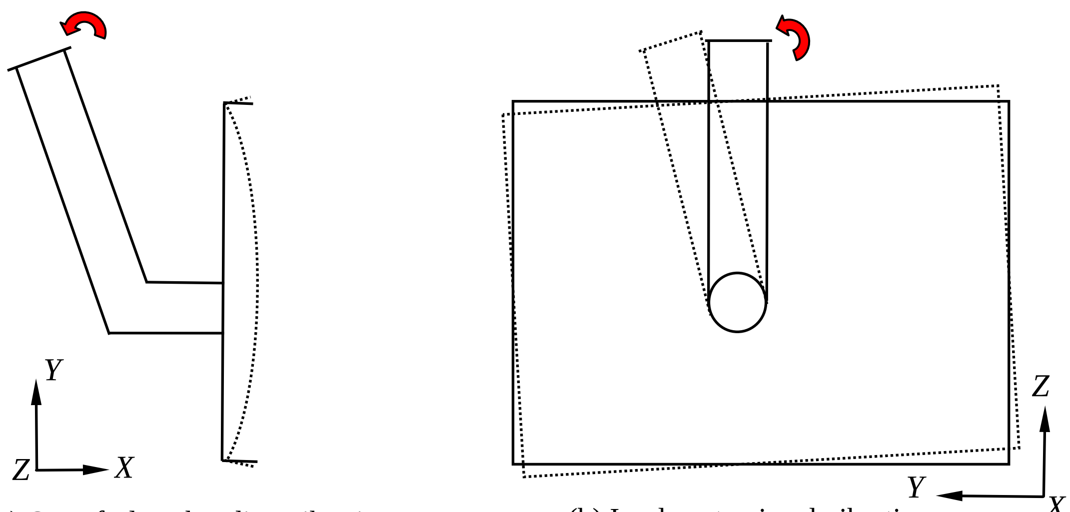

(a) Out-of-plane bending vibration (b) In-plane torsional vibration

Figure 3. Vibration modes of side wall of the tank

5.2. Seismic response mechanism of the turret-bushing assembly

For analysis of seismic responses of a turret-bushing assembly, a schematic model was proposed and illustrated in Figure 4. In the model, the turret-bushing assemblies of TT in *X* and *Y* directions and ST in *X* direction are simplified as a cantilever column with a rigid member bar at its base and a lumped mass point at its top. The position of the lumped mass point corresponds to the mounting flange of the bushing whereas the rigid member stands for the flange at roots of the turrets. To ensure that the rigid member can translate and rotate, translation-resistant and rocking-resistant springs at its two end were assumed. These springs simulate the constraints applied by the tank wall to the flanges at the roots of turrets.

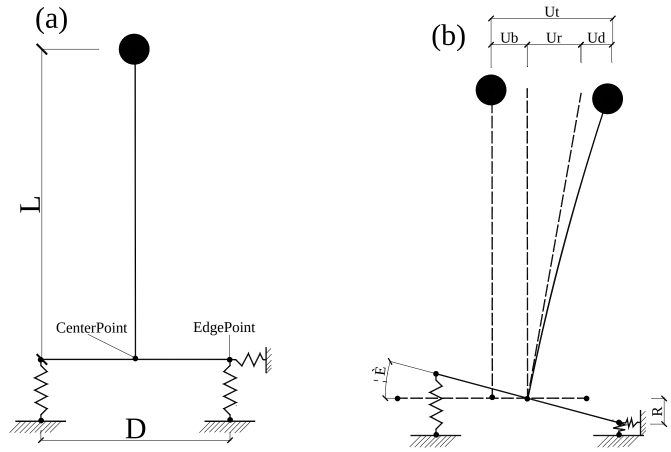

(a) Un-deformed model (b) Deformed model

Figure 4. Schematic diagram of bushing-turret assembly model

As shown in Figure 4, the total displacement (U_t) at the top of the turret, which is also the bushing flange, consists of translational displacement (U_b), rocking displacement (U_r), and deformed displacement (U_d). So U_t can be formulated as:

$$U_t = U_b + U_r + U_d \tag{2}$$

There are also certain geometrical relationships between rocking displacement (Ur) and rotational angle at the end of the rigid member:

$$U_r = L \times \theta \tag{3}$$

$$\theta = 2 R/D \tag{4}$$

$$U_t = U_b + 2L\frac{R}{D} + U_d \tag{5}$$

Where, R is the relative displacement between the center and edge of the flange at the turret root flange, θ is the angle of rotation of turret base flange, L is the length of turret projecting to the translation direction, and D is the outer diameter of the flange at the turret root flange.

Differentiating Eq. (5) twice gives an equation for the acceleration response:

$$\ddot{U}_t = \ddot{U}_b + 2L\frac{\ddot{R}}{D} + \ddot{U}_d \tag{6}$$

For the sake of convenience, Eq. (6) is rewritten as following:

$$A_t = A_b + L\frac{2A_R}{D} + A_d \tag{7}$$

Where, the accelerations : A_t, A_b, A_r, A_d are equal to $\ddot{U}_t, \ddot{U}_b, \ddot{R}, \ddot{U}_d$ and correspond to the displacements: U_t, U_b, R, U_d. In the shaking table tests, taking acceleration responses of SB in X direction for example, the accelerations A_t, A_b were obtained by accelerometers which were respectively attached to the mounting flange of bushing (AX5 in Figure 1.(b)) and the horizontal axis of symmetry for the flange at the bottom of the turret (AX6 in Figure 1.(b)). In addition, A_R is the difference of accelerations between the edge point (AX8 in Figure 1.(b) and axis of symmetry (AX6) of the flange at the base of turret. Accordingly, rocking acceleration component (A_r) and deformation acceleration component (A_d) can be expressed as:

$$A_R = A_{Edge\ point} - A_{center\ point} \tag{8}$$

$$A_r = L\frac{2A_R}{D} \tag{9}$$

$$A_d = A_t - A_b - A_r \tag{10}$$

The acceleration time histories for all components A_t, A_b, A_r, A_d and their corresponding FFT Fourier amplitude spectra in the case of WUX0.1g are plotted in Figure 5. It shows that for acceleration constituents at the top of turret (A_t), translational component (A_b) accounts for the largest component, which is followed by rocking component (A_r). The deformation component (A_d) represents the least component. When comparing to the input Wolong earthquake acceleration (A_e) in Figure 6 to the translational component (A_b) in Figure 5, it can be found that the plots of A_b and A_e are similar except that the amplitude of A_e is amplified to a certain extent by transformer tank and turret. For these acceleration Fourier amplitude spectra, when compared to A_b *and* A_e, A_r and A_d are concentrated frequency vibrations, with little correlation with A_e in terms of frequency components. From Fourier amplitude spectra, the shape Fourier amplitude spectrum of A_t around its peak coincides with that of A_r at the relevant frequency scope. Furthermore, the peak amplitude of the Fourier amplitude spectrum plot of A_r approximates that of A_t for ST in X direction. These observations suggest that the rocking vibration mainly contributes to the large vibration of the turret-bushing assembly in the corresponding frequency range, which significantly magnify the assembly acceleration responses.

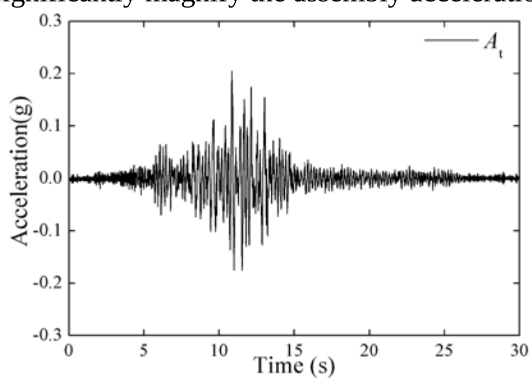

(a) Acceleration history of A_t

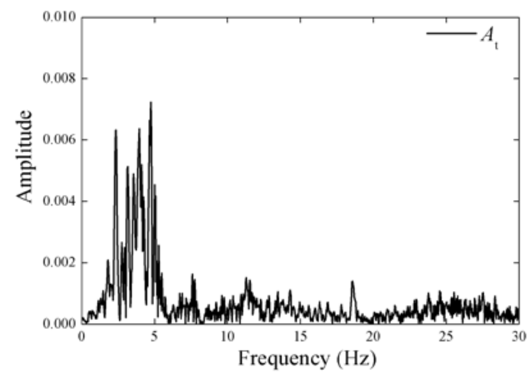

(b) Fourier amplitude spectrum of A_t

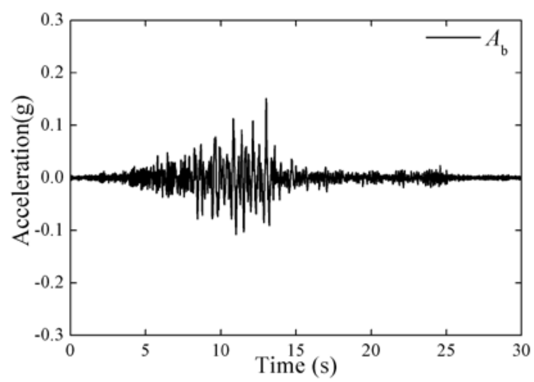

(c) Acceleration history of A_b

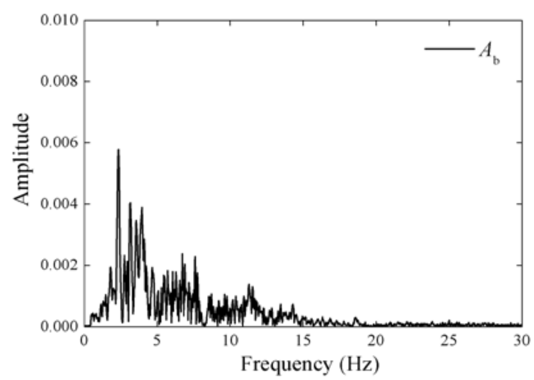

(d) Fourier amplitude spectrum of A_b

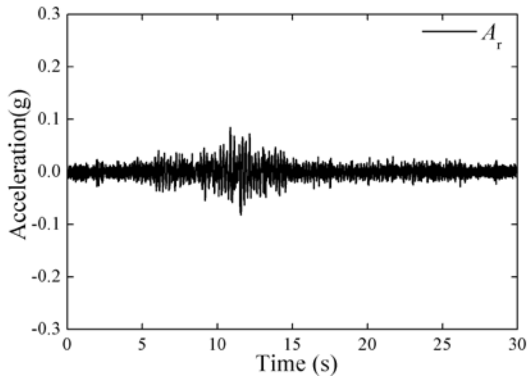

(e) Acceleration history of A_r

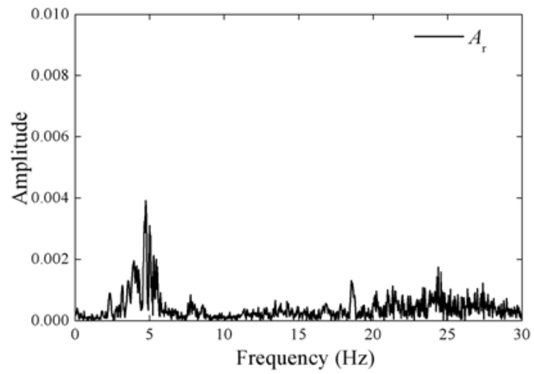

(f) Fourier amplitude spectrum of A_r

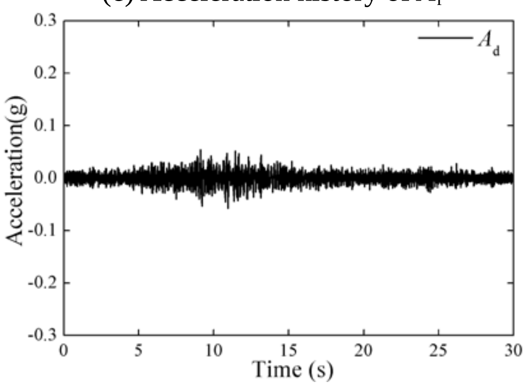

(g) Acceleration history of A_d

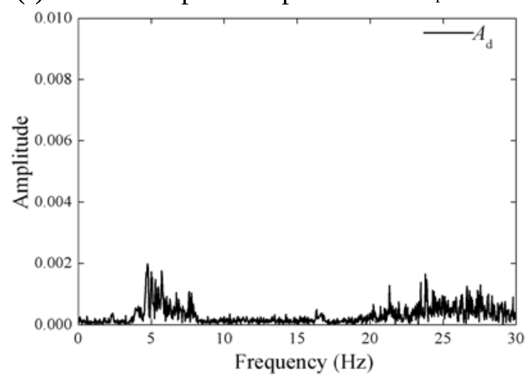

(h) Fourier amplitude spectrum of A_d

Figure 5. Constituents of acceleration at the top of ST in X direction in the case of WUX0.1g

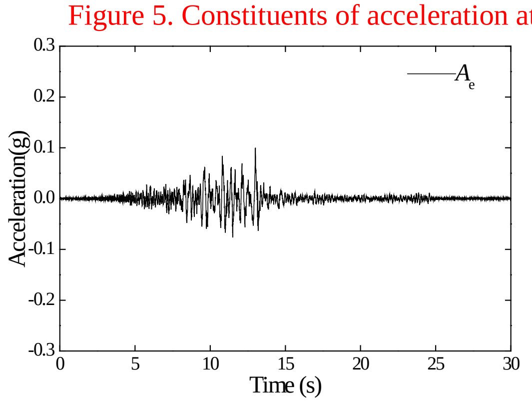

(a) Acceleration history of A_e

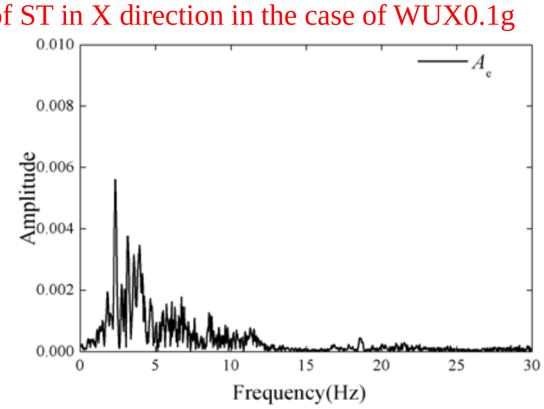

(b) Fourier amplitude spectrum of A_e

Figure 6. Time history and Fourier amplitude spectrum of input earthquake excitation in the case of WUX0.1g

5.3. Coupling effect between bushing vibration and turret rocking vibration

Figure 7 shows Fourier amplitude spectra for acceleration at the top of SB (A_{top}) and the corresponding rocking component (A_r) of the turret-bushing assembly in the case of WUX0.1g. It can be seen that the shape of Fourier amplitude spectra for A_{top} and corresponding rocking component (A_r) of the turret-bushing assembly resemble each other at the frequency around 5Hz, although the amplitude of Fourier amplitude spectrum for A_{top} is much larger than that of A_r of turret at the flange of SB. The spectral distribution of acceleration responses at the top bushing coincides with that of rocking acceleration component of the turret, which signifies that the bushing and turret rock together around the root of the turret. Therefore, there is a strong coupling effect between bushing vibration and turret rocking vibration.

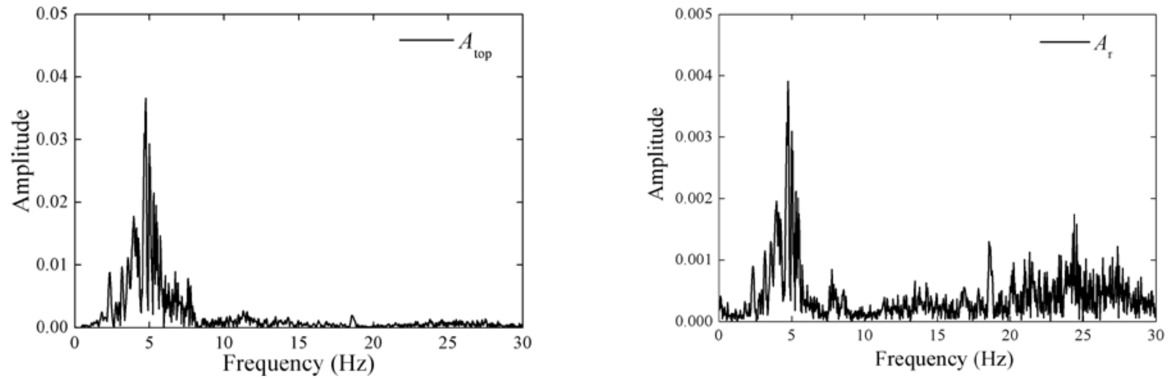

Figure 7. Comparison of Fourier amplitude spectra for acceleration at the top of SB and for rocking acceleration in the case of WUX0.1g

Based on the analysis above, it can be inferred that the main vibration mode of a bushing installed on a transformer and turret is the rocking vibration of turret-bushing assembly, and its fundamental frequency mainly depends on local bending stiffness of the tank side wall (or cover plate). These findings are quite different from the vibration pattern of a bushing fixed on a rigid stand, in which the main vibration pattern of a bushing is bending vibration and its fundamental frequency relies on its bending stiffness.

6. CONCLUSIONS

(1) Bushings seismic responses, such as acceleration, strain and displacement responses, are significantly magnified by the bushing-turret rocking vibration effect.

(2) The bending flexibility of the top plate and side wall of the transformer results in the out-of-plane bending vibration of the tank wall, which in turn leads to bushing-turret assembly rocking vibration around the turret bottom flange.

(3) There is a significant coupling effect between the bushing vibration and the turret rocking vibration, which accounts for fundamental frequency reduction and seismic response amplification of bushings.

7. References

[1] Xie Q, Zhu R Y (2011): Damage to electric power grid infrastructure caused by natural disasters in China-earthquake, wind and ice. *IEEE Power and Energy Magazine*, 9 (2): 28-36.

[2] You H B, Zhao F X (2013): M7.0 earthquake in Lushan and damage cause analysis of power facilities. *Electric Power Construction*, 34(8):100-104 (In Chinese).

[3] Evans N L, McGhie C (2011): The Performance of Lifeline Utilities following the 27th February 2010 Maule Earthquake Chile. *Proceedings of the Ninth Pacific Conference on Earthquake Engineering, Building an Earthquake-Resilient Society*, Auckland, New Zealand.

[4] Johnson F, Iliev K (2012). Earthquake effects on SDG&E's 500/230 kV imperial valley substation. IEEE Power and Energy Society General Meeting, San Diego, USA.

[5] Edwards CL (2012): Haiti Mw 7.0 Earthquake of January 12, 2010: Lifeline Performance. *ASCE Technical Council on Lifeline Earthquake Engineering*, Monograph No. 35.

[6] Kwasinski A, Eidinger J, Tang A, et al (2014): Performance of Electric Power Systems in the 2010-2011 Christchurch, New Zealand, Earthquake Sequence. *Earthquake Spectra*, 30 (1):205-230.

[7] Eidinger J, Davis C, Tang A, Kempner L (2012): M 9.0 Tohoku Earthquake March 11 2011 performance of water and power systems. G&E Engineering Systems Inc.

[8] Xie Q, Ma G L, Zhu RY, et al (2015): Shaking Table Test Research on Earthquake Response Mechanism of a Transformer-bushing System. *Proceedings of the CSEE*, 35(21): 5500-5510 (in Chinese).

[9] Whittaker A S, Fenves G L, Gilani A S J (2004): Earthquake performance of porcelain transformer bushings. *Earthquake Spectra*, 20(1):205-223.

[10] Ersoy S, Saadeghvaziri M A (2004): Seismic Response of Transformer-Bushing Systems. *IEEE transactions on power delivery*, 19(1):131-137.

[11] Filiatrault A, Matt H (2005): Experimental seismic response of high-voltage transformer -bushing systems. *Earthquake Spectra*, 21(4):1009-1025.

[12] Filiatrault A, Matt H (2006): Seismic response of high voltage electrical transformer-bushing systems. *ASCE Journal of structural engineering*, 132(2):287-295.

[13] Koliou M, Filiatrault A, Reinhorn A M (2013): Seismic response of high-voltage transformer-bushing systems incorporating flexural stiffeners I: Numerical study. *Earthquake Spectra*, 29(4):1335-1352.

[14] Koliou M, Filiatrault A, Reinhorn A M (2013): Seismic response of high-voltage transformer-bushing systems incorporating flexural stiffeners II: Experimental study. *Earthquake Spectra*, 29(4):1353-1367.

[15] IEEE Standard. 693-2005(2006): Recommended Practices for seismic design of substations. New York, USA.

[16] Li X J, Zhou Z H, Huang M, et al (2008): Preliminary Analysis of Strong-Motion Recordings from the Magnitude 8.0 Wenchuan, China, Earthquake of 12 May 2008. *Seismological Research Letters*, 79(6):844-854.

[17] GB 50260-2013 (2013): Code for seismic design of electrical installations. China Plan Press (In Chinese).